Acoustic recovery of lost power in pulse tube refrigerators

Article *in* The Journal of the Acoustical Society of America · February 1999

DOI: 10.1121/1.426262

3 authors, including:

Greg Swift
Swift Science and Engineering
163 PUBLICATIONS **6,539** CITATIONS

SEE PROFILE

Scott Backhaus
Los Alamos National Laboratory
136 PUBLICATIONS **6,519** CITATIONS

SEE PROFILE

Acoustic recovery of lost power in pulse tube refrigerators

G. W. Swift, D. L. Gardner, and S. Backhaus
Condensed Matter and Thermal Physics Group, Los Alamos National Laboratory, Los Alamos, New Mexico 87545

(Received 18 May 1998; accepted for publication 21 October 1998)

In an efficient Stirling-cycle cryocooler, the cold piston or displacer recovers power from the gas. This power is dissipated into heat in the orifice of an orifice pulse tube refrigerator, decreasing system efficiency. Recovery of some of this power in a pulse tube refrigerator, without sacrificing the simplicity and reliability inherent in a system with no cold moving parts, is described in this paper. In one method of such power recovery, the hot ends of both the regenerator and the pulse tube are connected to the front of the piston driving the refrigerator. Experimental data is presented demonstrating this method using a thermoacoustic driver instead of a piston driver. Control of time-averaged mass flux through the refrigerator is crucial to this power recovery, lest the refrigerator's cooling power be overwhelmed by a room-temperature mass flux. Two methods are demonstrated for control of mass flux: a barrier method, and a hydrodynamic method based on turbulent irreversible flow. At $-55\,^{\circ}\mathrm{C}$, the refrigerator provided cooling with 9% of the Carnot coefficient of performance. With straightforward improvements, similar refrigerators should achieve efficiencies greater than those of prior pulse tube refrigerators and prior standing-wave thermoacoustic refrigerators, while maintaining the advantages of no moving parts. [S0001-4966(99)00802-4]

PACS numbers: 43.35.Ud [HEB]

INTRODUCTION

As illustrated in Fig. 1(a) and (b), the orifice pulse tube refrigerator[1] (PTR) may be regarded as a Stirling refrigerator in which the cold moving parts have been replaced by stationary components. A reduction in efficiency may accompany this simplification in hardware, for a number of reasons. The most obvious cause of reduced efficiency is that work is absorbed and dissipated into waste heat in the orifice of the orifice PTR, whereas it is recovered at the cold piston of the Stirling machine and delivered back to the hot end of the system, either directly (via a displacer) or indirectly (via a crankshaft). Kittel[2] has shown that this orifice dissipation, regarded as a loss inherent to the orifice PTR, causes the coefficient of performance COP (i.e., the efficiency) of orifice PTRs to be bounded by T_C/T_H, significantly less than the Carnot COP $T_C/(T_H-T_C)$ which bounds Stirling refrigerators. (T is temperature and the subscripts C and H refer to cold and hot, respectively.) This inherent loss is most severe for $T_C \sim T_H$, thus far preventing practical use of orifice PTRs in noncryogenic applications such as food refrigeration and air conditioning. Orifice dissipation loss is also important in cryogenic systems: In one large orifice PTR with which we are familiar,[3,4] having 2 kW of cooling power at 125 K, orifice dissipation comprises 30% of the entropy generation and lost available work[5] in the refrigeration system (excluding losses in its thermoacoustic driver).

Acoustic transmission lines and inertances can pass acoustic power with little dissipation, while shifting the magnitude and phase of oscillatory pressure dramatically. This suggested to us that they could perform the work-recovery function of the Stirling's cold piston, while preserving the PTR's no-moving-parts advantage. This can be accomplished by at least two methods, illustrated schematically in Fig. 1(c) and (d) for a piston-driven pulse tube refrigerator. In the first method, an acoustic transmission line replaces the orifice, inertance, and compliance, connecting between the hot heat exchanger of the pulse tube and the back side of the drive piston. Most of the power that would previously have been dissipated in the orifice travels along the transmission line to the back side of the piston, helping move the piston and hence reducing the power required of the motor. In the second method, an inertance (or short transmission line) and a compliance between the piston and the aftercooler produce substantial amplitude and phase shifts between them, with the hot heat exchanger of the pulse tube connected at the *front* of the piston. In this method, the power previously dissipated in the orifice is delivered directly to the *front* of the piston and thereby added to the power supplied by the piston, reducing the power required of the motor. Thus, for both methods, system efficiency can be greater than for conventional orifice PTRs.

The fundamental idea behind these methods (and others) was fully anticipated over ten years ago by Ceperley,[6] whose early publications on ''traveling wave heat engines'' (including refrigerators) inspired the beginnings of thermoacoustics research here at Los Alamos. Ceperley realized that the essence of Stirling equipment is a regenerator in which the pressure and volumetric velocity oscillations are substantially in phase, and that an acoustic network with essentially toroidal topology [e.g., in our Fig. 1(c) or (d)] containing the Stirling heat-exchange components can provide such phasing. He showed that efficiencies near 80% of the Carnot efficiency are, in principle, possible with such configurations.

However, Ceperley did not discuss two features that we find are vital for practical operation of such refrigerators and

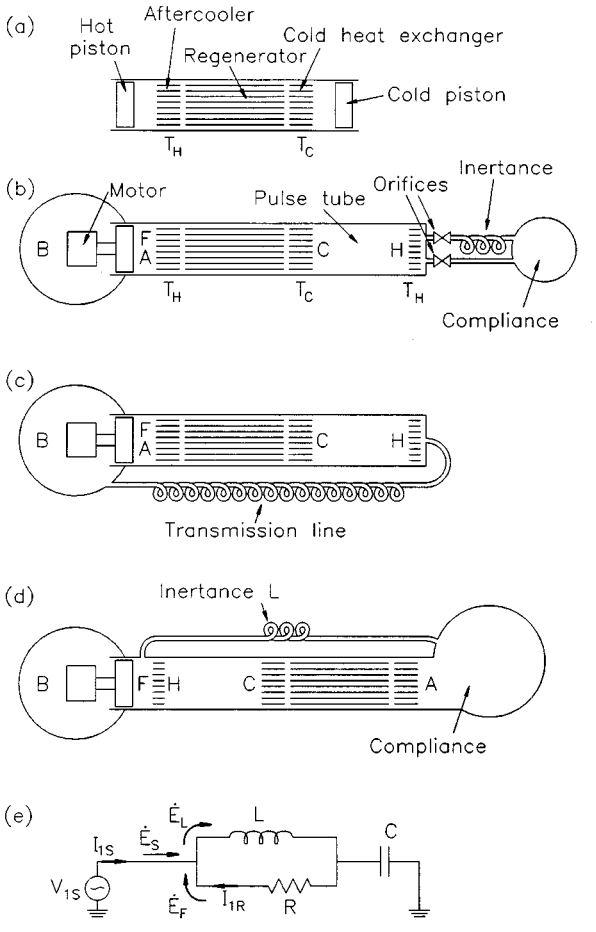

FIG. 1. Schematics of (a) Stirling cycle refrigerator (omitting details such as motor, crankshaft, etc.), (b) orifice pulse tube refrigerator, in which the cold piston of the Stirling cycle refrigerator is replaced by passive components, (c) pulse tube refrigerator with transmission-line feedback, and (d) pulse tube refrigerator with lumped boost configuration. To avoid confusion with the pulse tube's hot heat exchanger, the heat exchanger at the hot end of the regenerator is called the aftercooler. Capital letters in (b) through (d) label locations in the refrigerators: B—back of piston; F—front of piston; A—aftercooler; C—cold heat exchanger; H—hot heat exchanger; and L—inertance. The pistons move sinusoidally in time; the gas velocity in the regenerator is generally from aftercooler to cold heat exchanger while the pressure is high and generally in the opposite direction while the pressure is low. (e) Electric circuit crudely analogous to the acoustic network of (d).

engines. First, a thermal insulation column, namely the pulse tube itself in PTR practice, must insulate the ''remote'' heat exchanger (cold for refrigerators, hot for engines) from ambient temperature. The heat leak along a pulse tube can be as small as 5% of the cooling power of a PTR[7] using a tapered[8] pulse tube, although 15%–40% is typical.[9] Second, something must be done to prevent significant time-averaged mass flow from circulating around the torus. Gedeon[10] has discussed causes of such mass flow and the large heat flux it can carry.

To discuss these concepts quantitatively and in more detail, we take the essential physics to be spatially one-dimensional, with x specifying the coordinate along the direction of oscillatory gas motion. We use the conventional counter-clockwise phasor notation, so that time-dependent variables are expressed as

$$\xi(x,t)=\xi_m(x)+\mathrm{Re}[\xi_1(x)e^{i\omega t}], \tag{1}$$

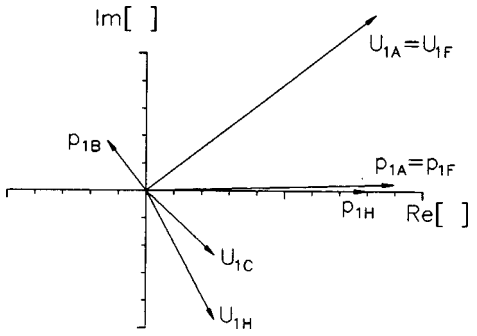

FIG. 2. Typical phasor diagram. Cryogenic pulse tube refrigerators with sufficient power to employ inertances have phasors similar to these, with p_1 in the pulse tube slightly smaller in magnitude than at the aftercooler, and usually lagging in phase; and with U_1 leading pressure at the aftercooler and lagging at both ends of the pulse tube. Pressure phasors are plotted as p_1/p_m, with each mark on the axes representing 0.01. Velocity phasors are plotted as U_1/Sa, where S is pulse tube area and a is sound speed, with each mark on the axes representing 0.001.

with the mean value ξ_m real, and with $\xi_1(x)$ complex to account for both the magnitude and phase of the oscillation. We adopt an acoustical point of view,[11] using the vocabulary of acoustic resistance, inertance, compliance, and transmission line to discuss the lumped and distributed impedances associated with the components of the PTR. This approach has been successful previously, even within regenerators.[12–15] In a minor departure from most prior PTR literature, which has focused on pressure p_1 and mass flux $\dot{M}_1$ as the oscillatory quantities of most interest, we will generally use the conventional acoustic variables p_1 and volumetric velocity U_1; the latter is related to mass flux simply via $\dot{M}_1=\rho_m U_1$, where ρ is the mass density. We take x and U_1 positive in the direction of positive acoustic power flow, for example to the right through the regenerators and pulse tubes in Fig. 1(a)–(c), and to the left through the transmission line in Fig. 1(c).

Some very general, almost unavoidable features of phasor diagrams for efficient cryogenic orifice PTRs are shown in Fig. 2, where the extra, capitalized subscripts on p_1 and U_1 correspond to the location labels in Fig. 1(b). We adopt the arbitrary convention that the phase of the pulse tube pressure is zero, so p_{1H} falls on the real axis. Typically the pressure drop along the pulse tube itself is immeasurably small, and that across the heat exchangers is negligible compared to that across the regenerator, which is in turn small compared to $|p_1|$, so $p_{1C}\cong p_{1H}$ and p_{1A} must lie close to p_{1H}, as shown in Fig. 2. Typically the time-averaged energy flux through the regenerator is small.[16] Applying energy conservation to the cold heat exchanger then shows that the cooling power $\dot{Q}_C$ is approximately equal to the total power flowing away from the cold heat exchanger in the pulse tube. The open nature of the pulse tube suggests that this total power flowing along it is the acoustic power $\frac{1}{2}\mathrm{Re}[p_1\tilde{U}_1]$, where the tilde signifies complex conjugation; in fact, heat can flow from hot to cold in the pulse tube, so the acoustic power is an upper bound of the cooling power:

$$\dot{Q}_{C,\mathrm{gross}}\leqslant \tfrac{1}{2}\mathrm{Re}[p_{1C}\tilde{U}_{1C}]. \tag{2}$$

Hence, in Fig. 1(a)–(d) acoustic power must flow in the di-

rection we have defined as positive x, so U_{1A}, U_{1C}, and U_{1H} must lie in the right half-plane in Fig. 2. An idealized refrigerator might be imagined with negligible entrained gas volume, so that U_1 would be independent of x in the pulse tube, $\rho_m U_1$ would be independent of x in the regenerator, and in particular the phase of U_1 would be constant throughout the refrigerator. As is well known,[1] nonzero gas volume causes x dependence in U_1, proportional to the compliance of the components and to $i\omega p_1$. This leads to a spread in phase of U_1 through the system, with U_1 at small x (i.e., toward the aftercooler) leading. The most efficient regenerator operation is achieved for the phase of p_1 falling somewhere between the phases of U_1 at the two ends of the regenerator. In orifice PTRs, this can be achieved using inertance[17,18] or a double inlet.[19] Viscous pressure drop occurs throughout the regenerator, so $p_{1A}-p_{1C}\cong p_{1A}-p_{1H}$ must be in phase with (parallel to) some weighted average of U_1 in the regenerator. Both $|U_1|$ and viscosity are highest at the regenerator's hot end, so the weighted average is dominated by U_{1A}, generally ensuring that p_{1H} lags p_{1A}. Finally, to the extent that the volume V_B on the back side of the piston is simply a compliance,

$$p_{1B}=j\frac{\gamma p_m}{\omega V_B}U_{1F}, \tag{3}$$

so p_{1B} must lead $U_{1F}=U_{1A}$ by 90°. Often the gas volume on the back side is large enough that $|p_{1B}|$ is much smaller than $|p_{1F}|$. These features are also illustrated in Fig. 2.

As discussed in the first paragraph, in an orifice PTR, the acoustic power

$$\dot{W}_H=\frac{\omega}{2\pi}\int_0^{2\pi/\omega}p(t)U(t)dt=\frac{1}{2}\mathrm{Re}[p_{1H}\tilde{U}_{1H}] \tag{4}$$

exiting the hot end of the pulse tube is lost, dissipated into heat in the orifice. This is typically nearly equal to the gross cooling power given in Eq. (2). To recover this acoustic power, thereby bringing the inherent efficiency limit of PTRs up to the Carnot limit, we can incorporate either of two low-loss acoustic connections shown in Fig. 1(c) and (d). The first method is described briefly in the next section: As shown in Fig. 1(c), a transmission line feeds the power recovered from the hot end of the pulse tube to the back side of the drive piston at p_{1B}. In Sec. II, we describe the second, more interesting method, shown in Fig. 1(d), in which the pulse tube delivers the recovered power directly to the front of the driver at p_{1F}, while the inertance delivers the drive power to the aftercooler. To convey the generality of the two methods, we describe them qualitatively for a piston driver in Secs. I and II, but we present experiments based on the second method using a thermoacoustic driver in Secs. III, IV, and V. In common with the double-inlet PTR,[19] both of these methods unfortunately permit second-order mass streaming through the refrigerator; in Sec. V we discuss our progress toward simple control of this important effect. Finally, in Sec. VI we present some conclusions and challenges for future development.

The idea that acoustic power will naturally circulate clockwise through the networks of Fig. 1(c) and (d) seems surprising, until we consider the LRC circuit of Fig. 1(e), a textbook electrical circuit crudely analogous to the acoustic network of Fig. 1(d). Many of us have derived expressions for the ac currents in each component of this circuit, but seldom do we consider the time-averaged electric power flows $\dot{E}$. By energy conservation, the time-averaged power $\dot{E}_S=\frac{1}{2}\mathrm{Re}[V_{1S}\widetilde{I_{1S}}]$ flowing from the voltage source into the circuit must equal the time-averaged power $\dot{E}_L-\dot{E}_F$ dissipated in the resistor. (In this idealized circuit, no time-averaged power can be absorbed in the dissipationless inductor L nor flow into the dissipationless capacitor C.) Ordinary ac circuit analysis easily yields the fed-back power

$$\dot{E}_F=\frac{1}{2}\mathrm{Re}[V_{1S}\widetilde{I_{1R}}]=\frac{|V_{1S}|^2}{2R}\frac{\omega^2LC(1-\omega^2LC)}{(1-\omega^2LC)^2+(\omega L/R)^2}, \tag{5}$$

with the sign convention as shown in the figure. Hence, whenever $\omega^2LC<1$, the directions of time-averaged power flow are as shown in the figure; positive electric power $\dot{E}_F$ flows *out* of the end of the resistor closest to the voltage source!

I. ACOUSTIC POWER RECOVERY

A. Transmission line configuration

Figure 1(c) illustrates an acoustic transmission line connecting the hot end of the pulse tube with the back side of the drive piston. A transmission line[20] obeys the equations

$$p_1(x)=p_{1i}\cos kx-i\frac{\rho_m a}{S}U_{1i}\sin kx, \tag{6}$$

$$U_1(x)=U_{1i}\cos kx-i\frac{S}{\rho_m a}p_{1i}\sin kx, \tag{7}$$

which show how p_1 and U_1 evolve with x along the transmission line, given their initial values p_{1i} and U_{1i} at $x=0$. The cross-sectional area of the transmission line is S, and a is the sound speed. [We omit the subscript m on variables such as a which, in principle, should be expressed as in Eq. (1) but whose oscillatory parts are of no interest in this work.] If the wave vector k is real, these equations describe a lossless transmission line, with $\frac{1}{2}\mathrm{Re}[p_1\tilde{U}_1]$ independent of x; losses in the transmission line (due to viscosity and thermal conductivity) can be included by using complex k.

From Eq. (6), a transmission line can connect the hot end of the pulse tube with the back side of the piston if its length l and area S are chosen such that

$$p'_{1B}=p_{1H}\cos kl-i\frac{\rho_m a}{S}U_{1H}\sin kl, \tag{8}$$

with the new value of p'_{1B} determined by a modified version of Eq. (3), accounting for the volumetric velocity flowing into V_B from the end of the transmission line:

$$p'_{1B}=j\frac{\gamma p_m}{\omega V_B}\left(U_{1F}-U_{1H}\cos kl+i\frac{S}{\rho_m a}p_{1H}\sin kl\right). \tag{9}$$

Because Eqs. (8) and (9) are complex, they represent four real equations in the four unknowns l, S, $\mathrm{Re}[p'_{1B}]$, and $\mathrm{Im}[p'_{1B}]$, so they will generally have a solution. The curves

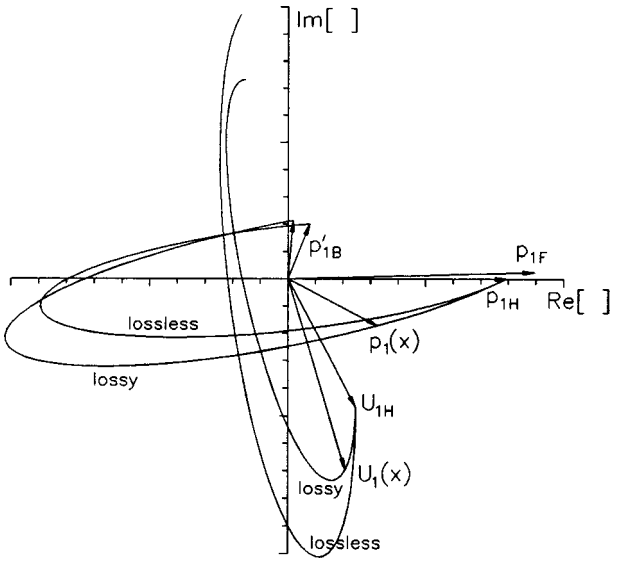

FIG. 3. Typical phasor diagrams for lossless (inner curves) and lossy (outer curves) transmission lines connected between pulse tube and back of piston. The transmission line's initial phasors p_{1H} and U_{1H} are the same as in Fig. 2.

in Fig. 3 illustrate Eqs. (6) and (7) when l and S are chosen correctly for the PTR whose phasors were shown in Fig. 2. The phasors are functions of x, following ellipses for the idealized, lossless (real k) transmission line; p_{1H}, U_{1H}, and S determine the eccentricity and orientation. The realistic, lossy transmission line yields similar curves, almost ellipses if the losses are sufficiently small, as shown in Fig. 3. Even for the lossy line, a substantial fraction of the acoustic power exiting the hot end of the pulse tube is delivered to the back of the drive piston, as shown by the reduction of the pressure difference across the piston from $p_{1F}-p_{1B}$ in Fig. 2 to $p_{1F}-p'_{1B}$ in Fig. 3. These figures are based on preliminary design calculations for a 100 K, helium-filled PTR having a gross cooling power of a few kW, which is typical of the cooling power we have been considering for liquefaction of natural gas.[3]

Although we decided to discuss this configuration here because it is easy to understand, we did not pursue it experimentally, because the more compact layout of the ''boost'' configuration discussed below was so appealing.

B. Lumped boost configuration

A second method to feed acoustic power from the hot end of the pulse tube back to the driver is illustrated in Fig. 1(d). The hot end of the pulse tube is connected directly to the front of the piston, while the aftercooler is connected through an acoustic network comprising an inertance and a compliance. We call this the ''lumped boost'' configuration because lumped acoustic impedances are used to boost $|p_{1A}|$ slightly above $|p_{1F}|$. (A ''distributed boost'' configuration, in which a short transmission line replaces the inertance and compliance, is also feasible.) In the lumped boost configuration, we will no longer neglect the flow resistance of the pulse tube's hot heat exchanger; its resistance R_H must be such that

$$p_{1H}-p_{1F}=R_H U_{1H}. \tag{10}$$

The compliance ensures that the volumetric velocity U_{1L} through the inertance differs from that at the aftercooler:

$$U_{1L}=U_{1A}+j\frac{\omega V_A}{\gamma p_m}p_{1A}, \tag{11}$$

where V_A is the volume of the compliance, so that the pressure difference across the inertance is

$$p_{1F}-p_{1A}=j\omega\frac{\rho_m l}{S}\left(U_{1A}+j\frac{\omega V_A}{\gamma p_m}p_{1A}\right), \tag{12}$$

where l and S are the length and area of the inertance. Taking the phasors at H and A to be given and combining Eqs. (10) and (12) to eliminate p_{1F}, we obtain a single complex equation in the unknowns R_H, V_A, l, and S, often with many possible solutions. Phasors for one such solution are shown in Fig. 4, where the refrigerator's end-point phasors are again the same as in Fig. 2.

The drive power is of course $\frac{1}{2}\,\mathrm{Re}[(p_{1F}-p_{1B})\widetilde{U_{1F}}]$ in both Fig. 1(b) and (d). If the compliance on the back side of the piston can be considered lossless, $\mathrm{Re}[p_{1B}\widetilde{U_{1F}}]=0$, so the drive power is simply $\frac{1}{2}\,\mathrm{Re}[p_{1F}\widetilde{U_{1F}}]$. In the lumped-boost case, $|U_{1F}|=|U_{1L}-U_{1H}|$ is rather large—much larger in Fig. 4 than in Fig. 2—so the amplitude of the piston motion in Fig. 1(d) must be much greater than in Fig. 1(b) or (c). Nevertheless, the power required of the piston is much less in Fig. 1(d) than in Fig. 1(b), because the phase angle between p_{1F} and U_{1F} is so large. Furthermore, the large magnitude of $|U_{1F}|$ presents no problem whatsoever if a pistonless thermoacoustic engine is used to drive the refrigerator.

II. APPARATUS

Encouraged by all these ideas, we proceeded to experiments with the lumped boost configuration. To use an existing driver[21] to power the experimental refrigerator, and to avoid the expense of building large hardware, we chose to test these ideas with a scale-model PTR that was approximately *similar*, in the technically strict sense of the word, to what would be required for a kW helium design. We built a ''half-scale'' PTR, filled with 2.4 MPa argon and operated at 23 Hz. It can be shown[22,23] that this is *similar* to a full-scale, 40-Hz, 3-MPa helium system, as long as the temperatures are high enough that argon can be regarded as an ideal gas. The physical phenomena and dimensionless combinations of variables in the half-scale argon PTR are all the same as at full scale in helium, just as a scale-model airplane in a wind tunnel and a full-sized airplane in flight share the same aerodynamics. The primary advantage of our half-scale argon model is that all powers are reduced by a factor of 16.7. A disadvantage is that we should keep this PTR's cold temperature greater than about 200 K, so that the argon is approximately an ideal gas. (Argon's critical point is 151 K, 4.9 MPa. At 2.4 MPa, it liquefies at 134 K.) Hence, our experiments can be regarded both as an easy exploration of some phenomena involved in acoustic recovery of otherwise

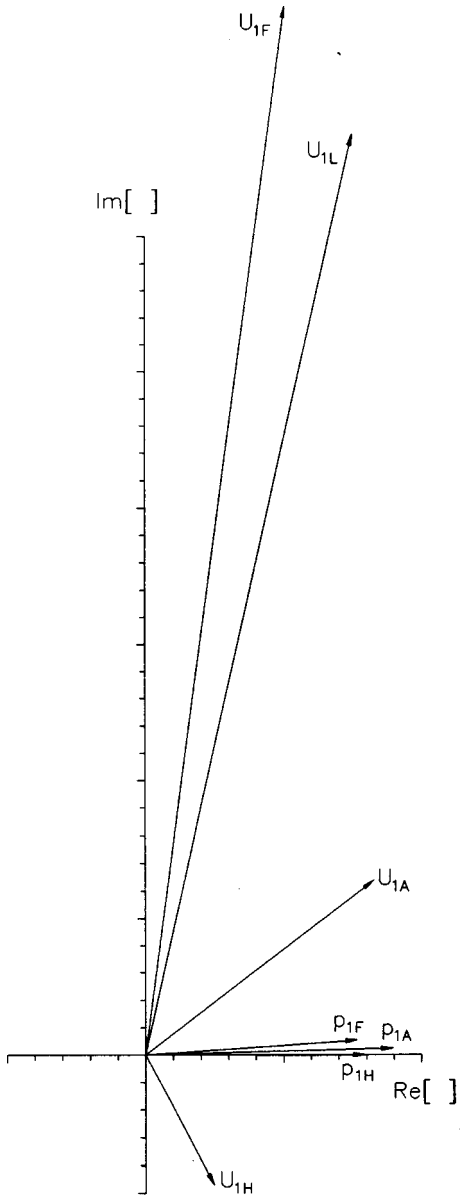

FIG. 4. Typical phasor diagrams for lumped boost configuration. The endpoint phasors p_{1H}, U_{1H}, p_{1A}, and U_{1A} are the same as in Fig. 2. The simple lumped impedances cause $p_{1H}-p_{1F}$ to be in phase with U_{1H}, $U_{1A}-U_{1L}$ to lag p_{1A} by 90°, and $p_{1F}-p_{1L}$ to lead U_{1L} by 90°.

lost power in PTRs, and as testing of an accurate scale model of a particular large refrigerator, with scaling details given in Table I.

In designing this hardware, we often sacrificed expected performance for versatility, ease of construction, and speed of design, because we correctly anticipated having to make many modifications in order to understand the behavior of such a novel apparatus. The system we built, illustrated in Fig. 5, is based on the lumped boost configuration of Fig. 1(d), but driven by a thermoacoustic engine instead of a piston and motor.

The heart of the refrigerator, its regenerator, was made of a 2.1-cm-thick stack of 400-mesh (i.e., 400 wires per inch) twilled-weave stainless-steel screens punched at 6.1-cm diameter. The total weight of the screens in the regenerator was 170 g. We calculated the hydraulic radius[24,25] of this

TABLE I. Scale factors to convert experimental data obtained with argon in this paper to numbers relevant to a larger helium-filled refrigerator. Multiply experimental data in this paper by the number in the table to obtain the expected result for the larger refrigerator. (Heat leaks that depend on the thermal conductivity of air, metal, or plastic do not scale.)

Variable	Multiplier
length	2
temperature	1
frequency	1.58
pressure	1.32
velocity	3.16
volumetric velocity	12.6
power	16.7

regenerator to be approximately 12 μm, based on its geometry and weight; in thermoacoustic calculations presented throughout the rest of this paper, we use 11 μm because this value gave the best agreement with our preliminary experiments in the ''traditional PTR'' configuration discussed below. The hydraulic radius is much smaller than the argon's thermal penetration depth (100 μm at 300 K), as required of a good regenerator. The stainless-steel pressure vessel around the regenerator had a wall thickness of 1.4 mm.

The pulse tube was a simple open cylinder, 3.0-cm id and 10.3 cm long, with 0.8-mm wall thickness. Its diameter is, of course, much greater than the argon's viscous penetration depth (90 μm at 300 K), and its length is greater than the 1-cm gas displacement amplitude in it at a typical operating point near $|p_1|/p_m \sim 0.1$. At each end, a few 35-mesh copper screens served as simple flow straighteners, to help maintain something resembling oscillatory plug flow in the pulse tube. We expected that argon's high density (relative to helium, which is almost universally used in PTRs) enhances the gravitational stability of this plug flow, so that careful flow straightening and tapering[8] would be unnecessary. This need for gravitational stability dictated the orientation of the refrigerator assembly with respect to vertical.

The cold heat exchanger between the regenerator and pulse tube was a 1.8-Ω length of NiCr ribbon wound zigzag on a fiberglass frame. Wires from the heater and a thermometer passed axially along the pulse tube to leak-tight electrical feedthroughs at room temperature. The two water-cooled heat exchangers (aftercooler and hot heat exchanger) were of shell-and-tube construction, with the Reynolds number of order 10^4 at $|p_1|/p_m \sim 0.1$ in the argon inside the 1.7-mm-diam, 18-mm-long tubes. The aftercooler had 365 such tubes, and the hot heat exchanger had 91.

The inertance was a simple metal tube with 2.2-cm id and 21-cm length, with 7-degree cones as shown in Fig. 5 at both ends to reduce turbulent end effects. The inertance and the refrigerator components were sealed to the flat plates above and below by rubber O-rings to enable easy modifications. The flat plates were held at a fixed separation by flange extensions and a cage of stout tubes through which long bolts passed, not shown in the figure. The compliance was half an ellipsoid with 2:2:1 aspect ratio, with a volume of 950 cm^3.

For simplicity, we insulated the cold parts of the apparatus with fiber-foam water-pipe insulation from the local

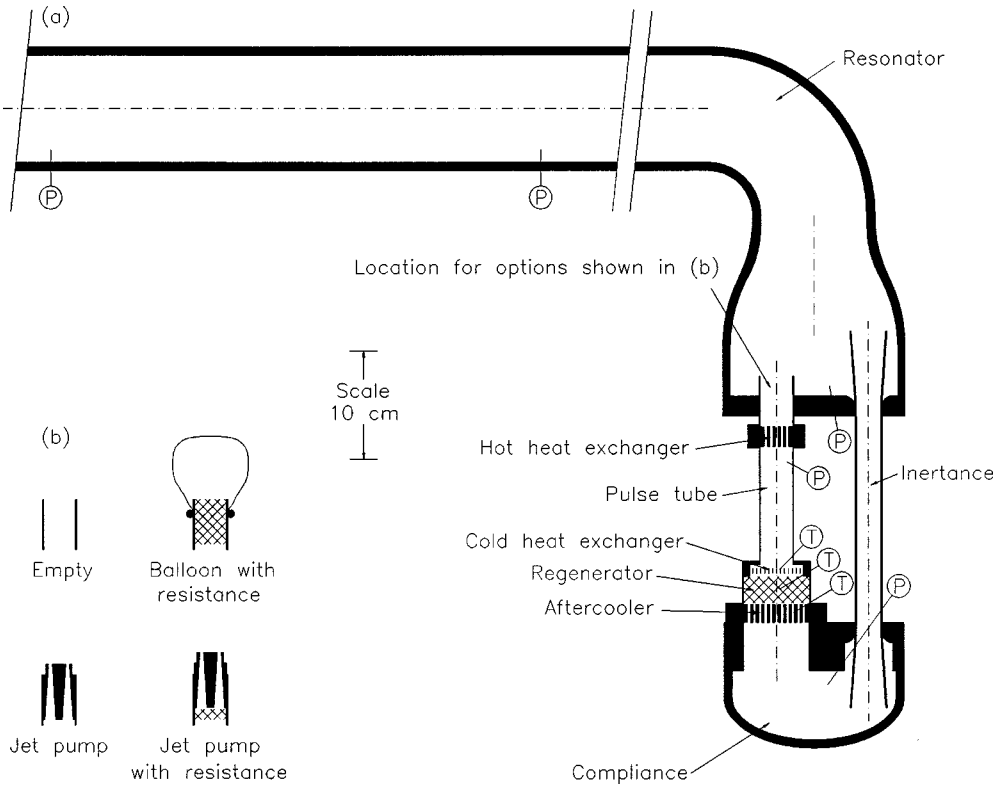

FIG. 5. (a) Drawing of the apparatus, in the inertance-boost configuration of Fig. 1(d). The dash–dot lines show local axes of cylindrical symmetry. Acoustic power circulates clockwise through the inertance and refrigerator part of the apparatus. ''P'' shows the location of a pressure sensor, and ''T'' the location of a temperature sensor. The heavy flanges around the aftercooler and hot heat exchanger contain water jackets. O-rings, most flanges, and bolts are omitted for clarity. The inside boundaries of the pressure vessel are to scale. (b) In the course of the measurements, these four options were used above the hot heat exchanger in (a). In each of the two cross-sectional views of the jet pump, two of the four tapered holes are shown.

hardware store. Type-K thermocouples measured temperatures in and near the regenerator. The 1.6-mm-diam thermocouple probe used to measure T_H was in the aftercooler, in the argon in one of the 365 tubes, touching the tube wall. The 0.8-mm-diam thermocouple probe used to measure T_C was standing freely in the argon between the cold heat exchanger and the flow straightener at the cold end of the pulse tube. Because of the different attachments of the T_C and T_H thermocouples, we believe that T_C represents the average temperature of the cold gas while T_H approximates the metal surface temperature in the aftercooler. The 0.8-mm-diam thermocouple probe whose temperature we will call T_{mid} was inserted into the very center of the regenerator, in a well that was drilled radially through the pressure-vessel wall and the screens. (Additional thermocouples outside the pressure vessel near the cold heat exchanger and the middle of the regenerator were used to confirm the internal temperature measurements.) Three piezoresistive pressure sensors (Endevco) in the compliance, pulse tube, and upper flat plate detected p_{1A}, p_{1H}, and p_{1F}, respectively, and two more sensors in the middle of the resonator were used to measure the acoustic power[26] flowing down the resonator from the thermoacoustic driver to the refrigerator. All pressure signals were detected with a lock-in amplifier.

A. First measurements

Preliminary measurements checked our implementation of the two-microphone acoustic-power measurement method[26] using the two sensors in the middle of the resonator. In these measurements, the PTR at the end of the resonator was replaced by a simple variable acoustic load comprising an adjustable valve R and a compliance C. Pressure sensors on either side of the valve allowed determination of the power dissipated in this RC network.[26] Figure 6 shows measurements of the two-microphone power as a function of dissipation in the RC network, at two pressure amplitudes in the resonator. The slopes in Fig. 6 are unity, demonstrating consistency between the RC and two-microphone methods. The region of large scatter in the measurements plotted in

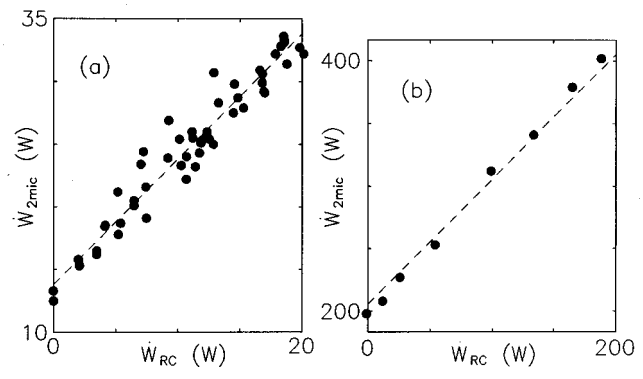

FIG. 6. Points show measured acoustic power $\dot{W}_{2\mathrm{mic}}$ passing the two-microphone location in the resonator, as a function of measured acoustic power $\dot{W}_{\mathrm{RC}}$ dissipated at the end of the resonator. For these preliminary measurements, an RC network replaced the refrigerator, inertance, and compliance of Fig. 5. The lines have slopes unity. (a) $|p_{1F}|/p_m = 0.038$ and (b) $|p_{1F}|/p_m = 0.094$.

Fig. 6(a) is due to thermoacoustic engine instability.[27] Fortunately, this instability was not encountered when the refrigerator was in place.

In Fig. 6(a) and (b), the offsets at zero RC dissipation are measures of the dissipation of acoustic power in that portion of the resonator between the two-microphone location and the RC network. This dissipation is up to four times greater than would be calculated for laminar acoustic dissipation, and is consistent with the turbulent dissipation calculations[28,29] of `DeltaE` Versions 3 and 4, assuming a pipe roughness factor of 1×10^{-3} for the resonator. This roughness factor is used in calculations of dissipation in the resonator and the inertance in the remainder of this paper.

To gain experience with our refrigerator, we made preliminary measurements with our PTR components (the regenerator, pulse tube, and three associated heat exchangers in Fig. 5) in the traditional PTR configuration shown in Fig. 1(b). Although PTR impedance networks at the hot end of the pulse tube are sometimes as simple as a single adjustable orifice and a compliance,[1] or a fixed lossy inertance and a compliance,[18] we used the configuration shown in Fig. 1(b), with two adjustable orifices (valves) and a fixed inertance in series with the compliance. The two valves allow independent control of both the magnitude and phase of the network's acoustic impedance.[21] In this traditional configuration, the refrigerator's performance was roughly as we had expected. At $|p_{1H}|/p_m=0.06$, the refrigerator cooled to $-115\,^{\circ}\mathrm{C}$ and had 20 W of net cooling power at $-50\,^{\circ}\mathrm{C}$; at $|p_{1H}|/p_m=0.08$ this cooling power was 40 W. Measurement of p_1 in the compliance and pulse tube, and knowledge of the gas volume in each component, allowed[21,28] us to infer U_1 throughout the refrigerator. The measured cooling power at $-50\,^{\circ}\mathrm{C}$ was about 10 W less than the inferred gross cooling power $\mathrm{Re}[p_{1H}\widetilde{U_{1C}}]/2$. We estimate that external heat leak contributes approximately half of this difference, with the balance due mostly to heat transport through the regenerator. In these preliminary measurements with the PTR in the traditional configuration, the most efficient operating points approached 5% of Carnot's coefficient of performance, using the net cooling power (i.e., electric resistance heater power, uncorrected for heat leak) and the two-microphone acoustic power in the calculations.

Next, we configured the refrigerator in the lumped boost configuration as shown in Fig. 5(a) [with the ''empty'' option of Fig. 5(b) installed above the pulse tube's hot heat exchanger]. The results were immediately disappointing: The refrigerator did not cool below 19 °C, essentially the temperature of the cooling water supplied to the water-cooled heat exchangers that day. (The aftercooler temperature $T_H=26\,^{\circ}\mathrm{C}$ for these measurements.) However, the pressure phasors seemed to be close to our expectations and the refrigerator's disappointing ''cold'' temperature was very strongly independent of heat load applied to the ''cold'' heat exchanger—e.g., at $|p_{1H}|/p_m=0.07$ an applied load of 70 W raised T_C to only 35 °C, as shown by the half-filled circles in Fig. 7. We concluded that the acoustic phenomena and gross cooling power were substantially as planned. Thus, we suspected that extremely vigorous streaming was effectively keeping the cold heat exchanger thermally anchored to the aftercooler, overwhelming the otherwise satisfactory thermoacoustic cooling power.

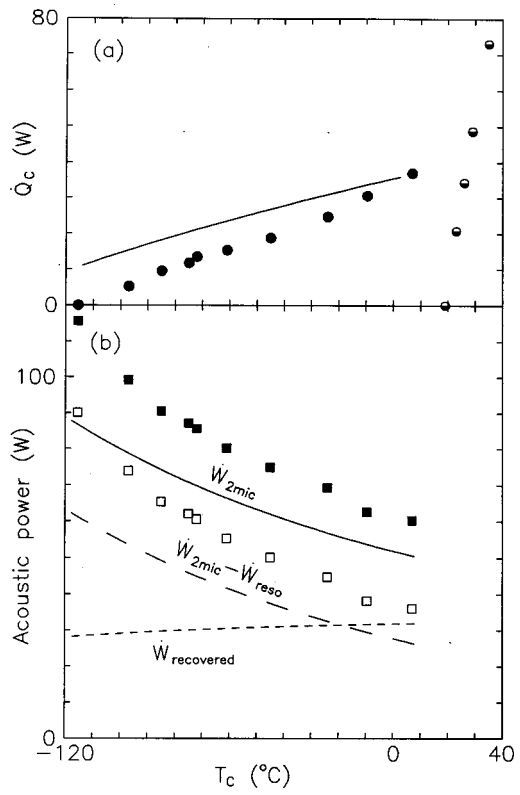

FIG. 7. Powers as a function of cold temperature T_C. The half-filled circles show measured cooling power with no balloon or other attempt to mitigate streaming ($|p_{1H}|/p_m=0.068$). The filled symbols and lines are with the balloon blocking streaming, at $|p_{1H}|/p_m=0.054$. (a) Cooling power. The experimental points show the electric power applied to the cold heat exchanger to maintain a given T_C. The line is the corresponding calculation. (b) Acoustic powers. The experimental points show measurements at the two-microphone location in the resonator; the solid line is the corresponding calculation. The open squares show the inferred acoustic power delivered to the refrigerator network, obtained by subtracting the calculated resonator dissipation from the measured two-microphone power. The long-dash line is the corresponding calculation. The short-dash line shows calculated values of recovered power (i.e., the acoustic power passing through the balloon).

III. SUPPRESSION OF STREAMING

A. Barrier method

It is essential that the time-averaged mass flow $\dot{M}$ through a PTR be near zero, to prevent a large steady energy flux $\dot{M}c_p(T_H-T_C)$ from flowing to the cold heat exchanger (where c_p is the gas' isobaric specific heat per unit mass). Such a steady energy flux would add an unwanted thermal load to the cold heat exchanger. In a traditional PTR configuration such as shown in Fig. 1(b), $\dot{M}$ is exactly zero; otherwise, mass would accumulate (or deplete, depending on sign) steadily in the compliance as a function of time. Gedeon[10] has discussed how nonzero $\dot{M}$ can arise in Stirling and pulse-tube cryocoolers whenever a closed-loop path exists for steady flow. Our lumped boost configuration clearly provides such a path; hence, we must understand and minimize $\dot{M}$.

Henceforth, we extend the complex notation introduced in Eq. (1) to second order by writing time-dependent variables as

$$\xi(x,t)=\xi_m(x)+\mathrm{Re}[\xi_1(x)e^{i\omega t}] + \xi_{2,0}(x)+\mathrm{Re}[\xi_{2,2}(x)e^{i2\omega t}]. \quad (13)$$

The final term, which oscillates at angular frequency 2ω, is of no interest here, but the time-averaged second-order term, with subscript ''2,0,'' is of great interest.

Gedeon argues that the second-order time-average mass flow

$$\dot{M}_2=\tfrac{1}{2}\mathrm{Re}[\rho_1\tilde{U}_1]+\rho_m U_{2,0} \quad (14)$$

is of primary concern. In acoustics, such second-order mass flow is known as streaming.[30] Gedeon shows that $\frac{1}{2}\mathrm{Re}[\rho_1\tilde{U}_1]=\rho_m\dot{W}_2/p_m$ in a regenerator, where $\dot{W}_2=\frac{1}{2}\mathrm{Re}[p_1\tilde{U}_1]$ is the acoustic power passing through the regenerator. Hence, $\frac{1}{2}\mathrm{Re}[\rho_1\tilde{U}_1]$ *must* be nonzero, and efficient regenerator operation requires that

$$U_{2,0}=-\tfrac{1}{2}\mathrm{Re}[\rho_1\tilde{U}_1]/\rho_m=-\dot{W}_2/p_m. \quad (15)$$

The consequences of ignoring this requirement can be severe. If $\dot{M}_2>0$, an undesired, streaming-induced heat load

$$\dot{Q}_{\mathrm{loss}}\sim\dot{M}_2 c_p(T_H-T_C) \quad (16)$$

flows from hot to cold through the regenerator. (If $\dot{M}_2<0$, such heat flows from hot to cold through the pulse tube, with equally harmful effect.) For $U_{2,0}=0$, the ratio of $\dot{Q}_{\mathrm{loss}}$ to the ordinary regenerator loss $\dot{H}_{\mathrm{reg}}$ is of the order of

$$\frac{\dot{Q}_{\mathrm{loss}}}{\dot{H}_{\mathrm{reg}}}\sim\frac{\gamma}{\gamma-1}\frac{(T_H-T_C)}{T_H}\frac{\dot{W}_H}{\dot{H}_{\mathrm{reg}}} \sim\frac{\gamma}{\gamma-1}\frac{(T_H-T_C)}{T_C}\frac{\dot{Q}_{C,\mathrm{gross}}}{\dot{H}_{\mathrm{reg}}}, \quad (17)$$

where $\dot{W}_H$ is the hot-end acoustic power and $\dot{Q}_{C,\mathrm{gross}}$ is the gross cooling power [see Eq. (2)]. In the third expression, each of the three fractions is >1 for cryocoolers; hence their product is $\gg 1$, and the unmitigated streaming-induced heat load would be much greater than the ordinary regenerator loss.

The steep slope $d\dot{Q}_C/dT_C$ shown in the half-filled circles in Fig. 7 provides an estimate of $\dot{M}_2$ in our refrigerator's ''empty'' configuration. Over the narrow temperature range of these data, gross cooling power and all other acoustic phenomena should be approximately constant and regenerator loss should be small, so the slope of the data should reflect Eq. (16): $-d\dot{Q}_{\mathrm{loss}}/dT_C=\dot{M}_2 c_p$. The experimental data yield $\dot{M}_2=9$ g/s. With Eq. (14) and our estimate that $\rho_m\dot{W}_2/p_m\sim 1$ g/s, this suggests that $\rho_m U_{2,0}$ was an order of magnitude larger than $\frac{1}{2}\mathrm{Re}[\rho_1\tilde{U}_1]$ for these measurements.

To quickly confirm our suspicion that the initial poor refrigerator performance shown as half-filled circles in Fig. 7 was due to such streaming, we installed a large rubber balloon (from a party-supplies store) above the pulse tube's hot heat exchanger, with the balloon protruding up into the resonator, as shown in Fig. 5(b). We rolled the balloon's collar completely up its neck and partly onto its body, so that tension in the rubber could not hold the balloon's surface against the sharp upper edge of the 3.1-cm-diam tube over which it was stretched. The balloon's limp volume was about 100 cm^3. We expected that this limp balloon would be acoustically transparent, but would block streaming flow completely.

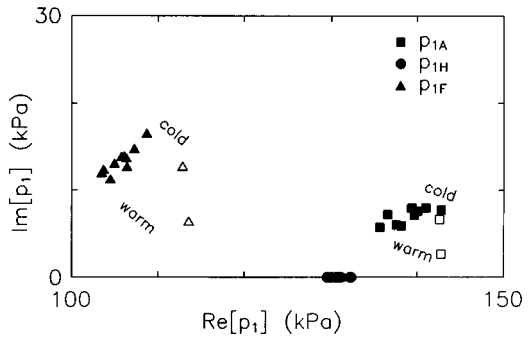

FIG. 8. Pressure phasors for measurements with balloon blocking streaming, at $|p_{1H}|/p_m=0.054$. The zero of phase has been chosen to set the phase of p_{1H} to zero, consistent with the other figures in this paper. The traditional phasor lines from the origin to each phasor have been eliminated to avoid clutter. Note the suppressed zero. The filled symbols are measurements; open symbols are calculations at the extreme values of T_C, with p_{1H} matched to the experimental values. The uppermost or rightmost symbols correspond to T_C near $-115\,^\circ$C; the lowermost or leftmost symbols correspond to T_C above $0\,^\circ$C.

At the same time, we installed extra resistance above the hot heat exchanger as shown in Fig. 5(b), because our earlier ''empty'' measurements had indicated that a larger flow resistance there was needed to make the phase of p_{1A} lead that of p_{1H}. The resistance comprised 130 g of 60 mesh copper screen packed into a volume 3 cm in diameter and 4 cm long. During fabrication, this screen was accidentally flattened and crushed to a higher density than expected, thereby providing more resistance than we wanted. Hence, we are uncertain of its hydraulic radius, which would otherwise have been approximately 100 μm. Fortunately, the system-performance calculations described below are not very sensitive to details in this component. We selected 60 μm as a reasonable estimate of the as-built hydraulic radius of this component, using this value in all calculations.

With the balloon in place, the refrigerator performed well, much like it had in the traditional PTR configuration described above, confirming our suspicion that enforcing $\dot{M}\equiv 0$ is the key to successful operation of this type of thermoacoustic system. The balloon survived without visible damage for 36 h of operation at $|p_{1H}|/p_m$ ranging from 0.04 to 0.10, more than enough time to obtain measurements.

In one set of measurements, we kept $|p_{1H}|/p_m=0.054$, while varying T_C from $-115\,^\circ$C to $7\,^\circ$C by adjusting the electric heater power $\dot{Q}_C$ at the cold heat exchanger. ($T_H=13\,^\circ$C throughout.) Figure 7 shows the resulting experimental cooling power and acoustic power requirements and Fig. 8 shows the experimental pressure phasors, together with some calculations of these and other variables. The calculations use `DeltaE`,[28] with geometry, mean pressure, fre-

TABLE II. The essential sequence of segments used in the DeltaE calculations described in this paper. (Free targets have been omitted for clarity.) The shooting-method guesses include T_m, complex p_1, and complex U_1 at the beginning, the complex branch impedance at the ''tbranch,'' and the heat flows at the aftercooler and cold heat exchanger. The shooting-method targets include T_H (at both aftercooler and hot heat exchanger), T_C, complex p_{1H}, the complex p_1 matching condition at the union, and the complex impedance at the ''hardend.''

	Segment type	Comment
0	BEGIN	at the two-microphone location
1	ISODUCT	long part of resonator
2	ISOCONE	conical adapter in resonator
3	ISODUCT	a little more resonator
4	TBRANCH	into the inertance
5	ISOCONE	cone at top of inertance
6	ISODUCT	the inertance
7	ISOCONE	cone at bottom of inertance
8	COMPLIANCE	the compliance
9	ISODUCT	short passage
10	TXFRST	aftercooler
11	STKSCREEN	regenerator
12	HXMIDL	cold heat exchanger
13	STKDUCT	pulse tube
14	TXLAST	hot heat exchanger
15	SXLAST	extra resistance
16	SOFTEND	terminates ''tbranch'' sequence
17	UNION	attaches 16 to the end of 3
18	HARDEND	ensures no U_1 leaks out

quency, p_{1H}, T_H, and T_C set to experimental conditions. (For those who are interested, Table II shows the sequence of DeltaE segments used in the calculations.)

In Fig. 8, p_{1F} and p_{1A} lead p_{1H}, with $|p_{1F}|<|p_{1H}|<|p_{1A}|$, consistent with the discussion leading up to Fig. 4. The measured and calculated phasors are in reasonably good agreement, showing that we understand the overall acoustic behavior of this network. Indeed, we can regard the complex differences $p_{1A}-p_{1H}$, $p_{1H}-p_{1F}$, and $p_{1F}-p_{1A}$ as indications of the impedances of the intervening components and the volumetric velocities through them [cf. Eqs. (10) and (12)]. From this viewpoint, the agreement between measured and calculated p_{1A} might be taken to indicate, for example, that we understand U_1 through the regenerator to within 10%–30% in magnitude and 10°–40° in phase.

In Fig. 7, the cooling power drops and the two-microphone acoustic power rises as T_C decreases. The calculations, which are in reasonable agreement with the experiments, provide insight to the main causes of these trends. First, the calculated gross cooling power $\dot{W}_C = \frac{1}{2}\mathrm{Re}[p_{1C}\tilde{U}_{1C}]$ is nearly constant at 40 W, independent of T_C, for these measurements. As discussed near Eq. (2), under the most ideal circumstances this would be the cooling power. The decrease in calculated $\dot{Q}_C$ below 40 W as T_C decreases is nearly proportional to T_H-T_C and is almost entirely due to heat flux through the regenerator. The difference between measured and calculated $\dot{Q}_C$ is also proportional to T_H-T_C, rising to 10 W at $T_C=-120\,°\mathrm{C}$. This could easily be due to a combination of ordinary heat leak through our insulation and streaming- or jet-driven convection in the pulse tube. Second, under the most ideal circumstances—with 40 W of cooling power and with Carnot's COP$=T_C/(T_H-T_C)$—the required net acoustic power would be $\dot{W}=(40\ \mathrm{W})(T_H-T_C)/T_C$, which rises from zero at $T_C=T_H$ to 35 W at $T_C=-120\,°\mathrm{C}$. This accounts for most of the 40 W rise in calculated $\dot{W}_{2\mathrm{mic}}$ with falling T_C in the figure. The measurements of $\dot{W}_{2\mathrm{mic}}$ exceed calculations by roughly 20%, for unknown reasons. Some 25 W of $\dot{W}_{2\mathrm{mic}}$ can be attributed to dissipation in the resonator between the two-microphone location and the refrigerator; this has been subtracted to yield the open squares and associated dashed line. Approximately 5 W of acoustic power is dissipated in the flow resistance under the balloon, 15 W is lost due to viscosity in the regenerator and adjacent heat exchangers, and 10 W is dissipated in the inertance.

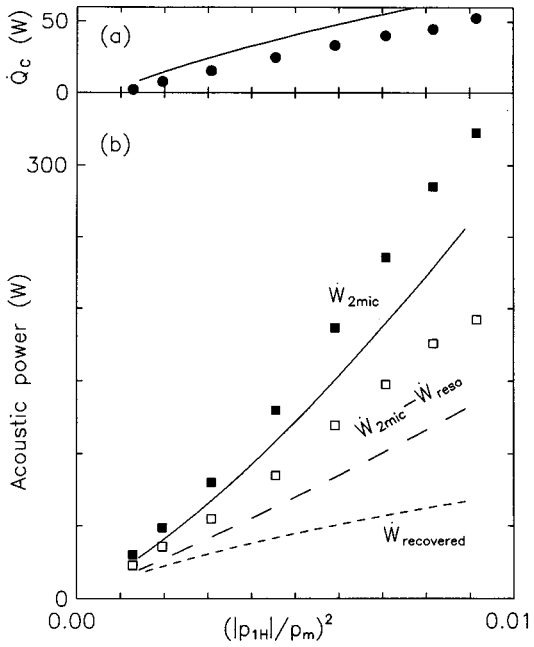

FIG. 9. Powers at $T_C=-60\,°\mathrm{C}$, as a function of pressure amplitude. (a) Cooling power. (b) Acoustic powers. The symbols have the same meaning as in Fig. 8.

If this were a traditional orifice PTR, $\dot{W}_C=40$ W would be dissipated in the orifice. In Fig. 7, the calculated fedback acoustic power $\dot{W}_{\mathrm{recovered}}$, which is of primary interest in this investigation, is near 30 W; hence, approximately 75% of $\dot{W}_C$ is recovered, fed back into the resonator. Note that, at the highest temperatures, $\dot{W}_{\mathrm{recovered}}$ is comparable to $\dot{W}_{2\mathrm{mic}}-\dot{W}_{\mathrm{reso}}$; in other words, at these temperatures feedback reduces the acoustic power delivered from the resonator to the refrigerator by roughly half.

In a second set of measurements with the balloon blocking streaming, we varied $|p_{1H}|$ while holding T_C constant near $-60\,°\mathrm{C}$. Unsurprisingly, the pressure phasors resembled those of Fig. 8 in phases and in degree of agreement between measurement and calculation. Cooling power and acoustic powers are displayed in Fig. 9. Again, calculations are in reasonably good agreement with experiment. Cooling power is proportional to $|p_{1H}|^2$, as expected. The difference between calculated and measured cooling power is roughly 5 W at the lowest amplitudes, consistent with the corresponding difference in Fig. 7; this difference increases at higher

amplitudes, for unknown reasons. The measurements of $\dot{W}_{2\mathrm{mic}}$ exceed calculations by roughly 20%, as they did in Fig. 7. At the highest amplitudes, resonator dissipation is a large fraction of $\dot{W}_{2\mathrm{mic}}$; subtracting resonator dissipation from $\dot{W}_{2\mathrm{mic}}$ leaves both calculated and measured $\dot{W}_{2\mathrm{mic}}$ proportional to $|p_{1H}|^2$, as expected. Again, the calculated $\dot{W}_{\mathrm{recovered}}$ is somewhat larger than the cooling power, is most of $\dot{W}_C$, and is large enough that in its absence the acoustic power $\dot{W}_{2\mathrm{mic}}-\dot{W}_{\mathrm{reso}}$ delivered from the resonator to the refrigerator would have to be significantly larger.

B. Hydrodynamic method

The measurements with the balloon convinced us that the acoustic aspects of the lumped-boost network were functioning as expected. However, we feared that the balloon would not be reliable enough for long-term practical use, so we returned our attention to the more challenging issue of streaming suppression. From among several options (including series bellows, fans, and parallel check valves) we chose to investigate asymmetry in hydrodynamic end effects to suppress streaming.

Gedeon[10] shows that $\dot{M}_2$ will be zero only if a nonzero $\Delta p_{2,0}$ exists across the regenerator, consistent with, and causing, the viscous flow of the correct $U_{2,0}$ in the regenerator. In a simple orifice PTR, this pressure difference appears automatically, because the topology imposes $\dot{M}_2=0$. However, when a regenerator is connected with other components in a ''loop'' topology, such as shown in Fig. 1(c) or (d) or such as in a double-inlet PTR, the topology does not ensure $\dot{M}_2=0$; rather, it ensures that $\oint(dp_{2,0}/dx)dx=0$ around the loop. To obtain the correct $U_{2,0}$ in the regenerator in ''loop'' systems, we must design the other components of the loop so that they impose the correct $\Delta p_{2,0}$ across the regenerator.

The required $\Delta p_{2,0}$ can be estimated using the low-Reynolds-number limit of Fig. 7-9 of Kays and London[25]

$$\frac{dp}{dx}\simeq-\frac{6U\mu}{Sr_h^2} \tag{18}$$

for the pressure gradient in a screen bed of cross-sectional area S and hydraulic radius r_h, where U is the volumetric velocity and μ is the viscosity. (The numerical factor depends weakly on the volumetric porosity of the bed.) With Eq. (15) for U, this yields

$$\Delta p_{2,0}\simeq\frac{6}{Sr_h^2p_m}\int_{\mathrm{reg}}\mu_m(x)\dot{W}_2(x)dx \tag{19}$$

for the pressure difference across the regenerator when $\dot{M}_2\equiv0$. (The viscosity's x dependence is due to the temperature gradient.) For our apparatus at typical operating conditions, $\Delta p_{2,0}$ is of the order of a few hundred Pa.

In the limit of low viscosity or large tube diameters and in the absence of turbulence, $p_{2,0}$ would be described by some acoustic version of the Bernoulli equation. This suggests that an acoustically ideal loop connecting the two ends of the regenerator would impose across the regenerator a pressure difference of the order of $\Delta[\rho_m u_1\tilde{u}_1]$, where u_1 is the complex velocity amplitude. (Such an ideal loop might include a pulse tube, transmission line, and compliance, without heat exchangers or other components with small passages.) This pressure difference is typically much smaller than the $\Delta p_{2,0}$ given in Eq. (19) that is required for $\dot{M}_2=0$. Hence, to produce the required $\Delta p_{2,0}$, we need an additional physical effect or structure in the loop, relying on turbulence, viscosity, or some other physical phenomenon not included in the Bernoulli equation.

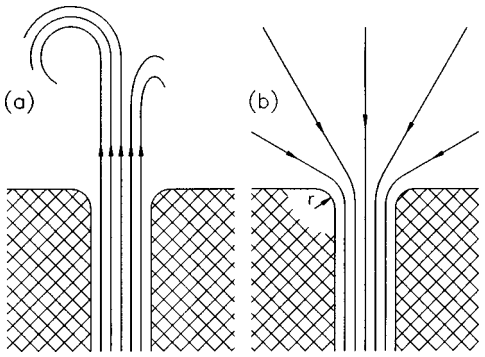

FIG. 10. Illustration of asymmetric flow at high Reynolds number at the transition between a small tube and open space. (a) Outflow. (b) Inflow, for which the radius r of rounding of the lip is important.

Asymmetry in hydrodynamic end effects can produce this required $\Delta p_{2,0}$. In a tapered transition between a small-diameter tube, where $|u_1|$ is large, and a large-diameter tube, where $|u_1|$ is small, turbulence would be avoided and Bernoulli's equation would hold if the taper were sufficiently gentle. At the opposite extreme, for an abrupt transition, we expect large $|u_1|$ to generate significant turbulence, and further we expect the oscillatory pressure drop across the transition to reflect the phenomena known as ''minor losses''[31] in high-Reynolds-number steady flow. If the gas displacement amplitude is much greater than the tube diameter, we also expect that the flow would at any instant have little memory of its past history, so that the acoustic behavior can be deduced from careful time integration of the steady-flow phenomena.

Ideally, the pressure at each instant of time could be described by the ordinary, steady-flow Bernoulli equation. At abrupt transitions, deviations of the pressure from this ideal are called ''head loss'' or ''minor loss'' in steady flow, with the lost pressure Δp_{ml} given by

$$\Delta p_{ml}=K\,\tfrac{1}{2}\rho u^2, \tag{20}$$

where K is the minor-loss coefficient, which is well known[31,32] for many transition geometries, and u is the velocity. For our purposes, the most important fact about K is that it depends strongly on the direction of flow through the transition. In the example shown in Fig. 10, a small tube is connected to an essentially infinite open space. When the gas (at velocity u inside the tube) flows out of the tube, a jet occurs, and kinetic energy is lost to turbulence downstream of the jet; $K_{\mathrm{out}}=1$. In contrast, when gas flows into the tube, the streamlines in the open space are widely and smoothly dispersed; K_{in} varies from 0.5 to 0.04, with smaller values for larger radius r of rounding of the edge of the entrance.

If $u=|u_1|\sin\omega t$, we can calculate the time-averaged pressure drop by integrating Eq. (20) in time:

$$\overline{\Delta p_{ml}}=\frac{\omega}{2\pi}\left(\int_0^{\pi/\omega}K_{\rm out}\frac{1}{2}\rho|u_1|^2\sin^2\omega t dt - \int_{\pi/\omega}^{2\pi/\omega}K_{\rm in}\frac{1}{2}\rho|u_1|^2\sin^2\omega t dt\right)$$
$$=\tfrac{1}{8}\rho|u_1|^2(K_{\rm out}-K_{\rm in}). \quad (21)$$

This is the source of $\Delta p_{2,0}$ that we will use. Such simple control of $\dot{M}_2$ is not without penalty, however; acoustic power is dissipated at a rate

$$\dot{E}=S\frac{\omega}{2\pi}\int_0^{2\pi/\omega}\Delta p_{ml}u dt$$
$$=S\frac{\omega}{2\pi}\left(\int_0^{\pi/\omega}K_{\rm out}\frac{1}{2}\rho|u_1|^3\sin^3\omega t dt - \int_{\pi/\omega}^{2\pi/\omega}K_{\rm in}\frac{1}{2}\rho|u_1|^3\sin^3\omega t dt\right)$$
$$=\frac{1}{3\pi}\rho|u_1|^2|U_1|(K_{\rm out}+K_{\rm in}) \quad (22)$$
$$=\frac{8}{3\pi}\overline{\Delta p_{ml}}|U_1|\frac{K_{\rm out}+K_{\rm in}}{K_{\rm out}-K_{\rm in}}, \quad (23)$$

where S is the area of the small tube. Equation (23) shows that the best way to produce a desired $\overline{\Delta p_{ml}}$ is to insert the device at a location where $|U_1|$ is small, and to shape it so that $K_{\rm out}-K_{\rm in}$ is as large as possible.

In our refrigerator, $|U_1|$ is smallest at the cold heat exchanger, but that is an unsuitable location for adding a dissipative structure. The hot heat exchanger has only slightly larger $|U_1|$, and already requires some extra dissipation to ensure that p_{1A} leads p_{1H} slightly, so we chose the space above the hot heat exchanger, previously occupied by the balloon and extra resistance, as the location for our experiments on asymmetry in end effects for streaming control. We installed what we call the ''jet pump,'' a brass block bored through with four identical tapered holes, each 5.3 cm long, 10 mm diam at the lower end, and 4 mm diam at the upper end, as shown in Fig. 5(b). We expected that end effects at the small ends of the holes would be strongly asymmetric, causing the desired $\overline{\Delta p_{ml}}$, while the velocities at the large ends of the holes would be small enough that minor losses would be negligible and the tapers joining the ends would be gradual enough to prevent minor losses in between.

To investigate the control of $\overline{\Delta p_{ml}}$ through the dependence of $K_{\rm in}$ on the radius r of rounding of the entrance, we made a series of temperature measurements with the jet pump in our refrigerator, at $|p_{1H}|/p_m\simeq 0.06$ with no heat applied at the cold heat exchanger, with each measurement having a different entrance rounding at the small ends of the tapered holes in the jet pump. At this pressure amplitude, the Reynolds number of the oscillatory flow was 2×10^5 and the gas displacement amplitude $|U_1|/\omega S\sim 0.2$ m at the jet. The results of this series of temperature measurements are shown

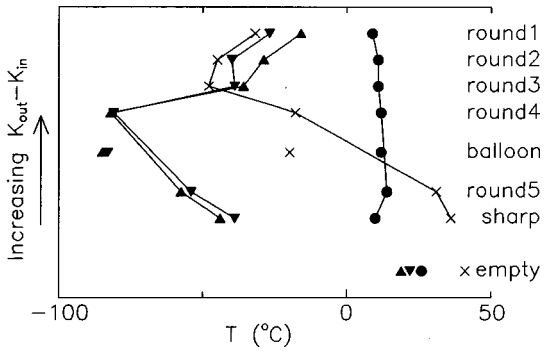

FIG. 11. Temperatures in and near the regenerator as the hardware above the hot heat exchanger was changed. Circles, aftercooler temperature T_H; ×, mid-regenerator internal temperature $T_{\rm mid}$; erect triangles, cold heat exchanger internal temperature T_C; inverted triangles, cold heat exchanger external temperature. Lines link the six jet-pump data sets, which are arranged vertically in order of increasing strength of jet pump. Measurements under comparable conditions with the balloon and with no attempt to mitigate streaming (''empty'') are inserted into the sequence at appropriate vertical locations.

in Fig. 11. We began this tedious process with sharply machined edges (''sharp'' in Fig. 11) at the small ends of the four holes. Next, we rounded and polished the edges of the holes to $r\sim 0.5$ mm (''round1''), and then we proceeded to machine away ~ 0.1 mm at a time from the flat upper end of the jet pump (''round2'' through ''round5''), thus removing ever more of the rounded edges and returning the entrances ever closer to ''sharp.'' Also shown for comparison in the figure are data from the balloon measurements and from our preliminary measurements with no attempt to mitigate streaming [corresponding to the ''empty'' configuration of Fig. 5(b) and the lowest half-filled circle in Fig. 7].

Figure 11 is qualitatively consistent with the discussion of streaming and its control presented above, and in particular with the expected increase of $\overline{\Delta p_{ml}}$ with decreasing $K_{\rm in}$ as determined by the radius of rounding of the entrances. With no attempt to control streaming (''empty''), the cold and hot temperatures T_C and T_H were nearly equal, and the temperature $T_{\rm mid}$ in the middle of the regenerator was 20° warmer than the others. In this circumstance, $\dot{M}$ was large and positive (i.e., flowing through the regenerator from hot to cold). With such large $\dot{M}$, the middle of the regenerator was thermally tied to the average gas temperature on the hot end of the regenerator (which happened to be about 20° warmer than the aftercooler metal surface temperature T_H), and this warm gas flowing up through the regenerator delivered a large heat load to the cold heat exchanger, as implied by Eq. (17), keeping T_C high. With the ''sharp'' and ''round5'' versions of the jet pump, a nonzero $\overline{\Delta p_{ml}}$ reduced $\dot{M}$, thereby lowering the temperatures. With the ''round4'' version of the jet pump, we were fortunate to arrive at the value of $K_{\rm in}$ that generated exactly the $\overline{\Delta p_{ml}}$ needed to force $\dot{M}\simeq 0$, so the temperatures were very nearly equal to those we observed when the balloon enforced $\dot{M}\equiv 0$. More well-rounded versions of the jet pump (''round3'' through ''round1'') reduced $K_{\rm in}$ and hence generated even greater $\overline{\Delta p_{ml}}$, causing $\dot{M}<0$; in these cases, the cold heat exchanger was loaded by warm gas flowing down through the pulse tube, and the mid-

regenerator temperature felt the thermal influence of gas flowing steadily from the cold end of the regenerator.

Furthermore, the phase of p_{1A} increased steadily from ''round1'' through ''round5'' and ''sharp,'' consistent with the increase in the effective resistance to U_1 of the jet pump with increasing K_{in} that we expect based on Eq. (22).

Hoping that we understood all the important features of this apparatus, we made final modifications. We upgraded our computer model of the apparatus to incorporate the minor losses of Eq. (22), both at the small end of the jet pump and at both ends of the inertance. The model results suggested that system performance would be improved if we added some extra resistance above the hot heat exchanger, so we inserted 25% of our copper screen resistance under the jet pump; together with the resistance of the jet pump itself, this provided a total resistance that left p_{1A} nearly in phase with p_{1H} and yielded calculated performance superior to that we had observed with the balloon. We rounded and polished the jet pump hole entrances again, repeating abbreviated measurements of temperatures and iteratively smoothing the entrances until we returned to temperatures comparable to ''round4'' in Fig. 11. We then proceeded with more extensive measurements.

In one set of measurements with this final jet-pump configuration, we kept $|p_{1H}|/p_m = 0.054$ while varying T_C by adjusting the electric heater power $\dot{Q}_C$ at the cold heat exchanger. These conditions are comparable to those for the ''balloon'' and ''empty'' data shown in Fig. 7. The results are shown in Fig. 12. The mid-regenerator temperature was 20 °C for $T_C = -80$ °C, indicating that the jet pump was too weak, with nonzero $\dot{M}$ flowing from hot to cold through the regenerator. Nevertheless, the cooling power is far greater than it was for the ''empty'' data, showing that the jet pump was far better than nothing at suppressing streaming. At high T_C the calculated and measured cooling powers are in good agreement; here, a small nonzero $\dot{M}$ has less effect on the net cooling power. At lower T_C the measured cooling power is significantly lower than the calculated values (and lower than the balloon measurements), as the small nonzero $\dot{M}$ consumes a significant fraction of the cooling power. The acoustic powers are negligibly affected by small $\dot{M}$, so the agreement between measured and calculated $\dot{W}_{2\text{mic}}$ is as good as it was for the balloon measurements. Both calculated cooling power and calculated $\dot{W}_{2\text{mic}}$ are better than for the balloon case, because of the better choice of total flow resistance above the hot heat exchanger discussed in the previous paragraph.

In a second set of measurements, we varied $|p_{1H}|$ while holding T_C constant near -55 °C; these conditions are comparable to the balloon measurements shown in Fig. 9. The results are shown in Fig. 13. In Fig. 13(a), the experimental cooling power exhibits interesting structure, which we believe is due to nonzero $\dot{M}$. A local maximum in $\dot{Q}_C$ occurs at $(|p_{1H}|/p_m)^2 = 0.0025$, for which $T_{\text{mid}} = 10$ °C as shown in Fig. 13(c). This value of T_{mid} is comparable to that we observed with the balloon at this T_C, suggesting that $(|p_{1H}|/p_m)^2 = 0.0025$ happens to obtain $\dot{M} \simeq 0$ with this jet

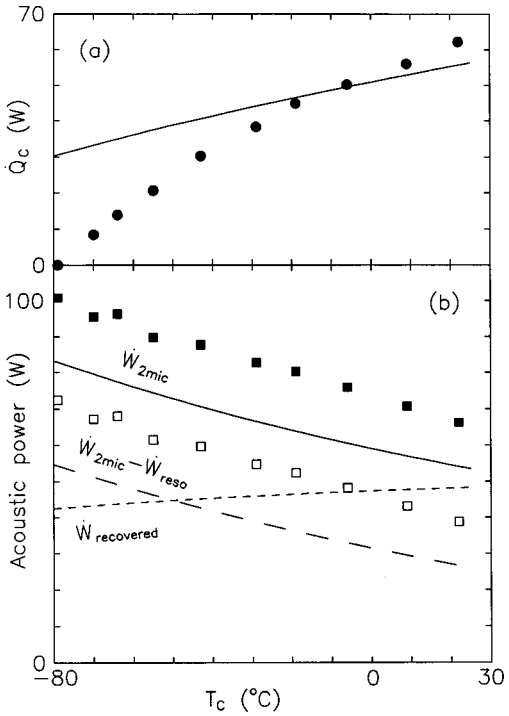

FIG. 12. Powers as a function of cold temperature T_C, with final configuration with jet pump and small extra resistance, at $|p_{1H}|/p_m = 0.054$. $T_H = 12$ °C throughout. (a) Cooling power. The experimental points show the electric power applied to the cold heat exchanger to maintain a given T_C. The line is the corresponding calculation. (b) Acoustic powers. The experimental points show measurements at the two-microphone location in the resonator; the solid line is the corresponding calculation. The open squares show the inferred acoustic power delivered to the refrigerator network, obtained by subtracting the calculated resonator dissipation from the measured two-microphone power. The long-dash line is the corresponding calculation. The short-dash line shows calculated values of the recovered power (i.e., the acoustic power passing through the balloon).

pump r. At lower $|p_{1H}|$, the T_{mid} measurements imply $\dot{M} < 0$; at higher $|p_{1H}|$, they imply $\dot{M} > 0$. In both cases, cooling power is reduced significantly by this streaming. The experimental acoustic power $\dot{W}_{2\text{mic}}$ in Fig. 13(b) is in reasonable agreement with calculations over the whole range of $|p_{1H}|$, with no obvious feature near the $\dot{M} \simeq 0$ amplitude, again confirming our expectation that nonzero $\dot{M}$ has little effect on purely acoustic phenomena.

However, the dependence of $\dot{M}$ on amplitude implied by Fig. 13 suggests that our understanding is incomplete: Eq. (19) for the pressure difference required across the regenerator and Eq. (21) for the pressure difference produced by the jet pump are both quadratic in amplitude, so if they conspire to make $\dot{M} \simeq 0$ at one amplitude, then they should do so at all amplitudes. Furthermore, there is a significant difference between the results of these two equations. Using calculated powers and velocities at $(|p_{1H}|/p_m)^2 = 0.0025$ in Fig. 13, Eq. (19) yields 200 Pa while Eq. (21) yields 2 kPa (assuming $K_{\text{out}} - K_{\text{in}} \sim 0.7$). Rough estimates show that a large number of other components and phenomena in the apparatus may each contribute tens to hundreds of Pa to $\oint (dp_{2,0}/dx)dx$. Representative examples include the gravitational head due to the cold gas in the cold components, minor losses at the inertance ends, boundary-layer streaming in the inertance,

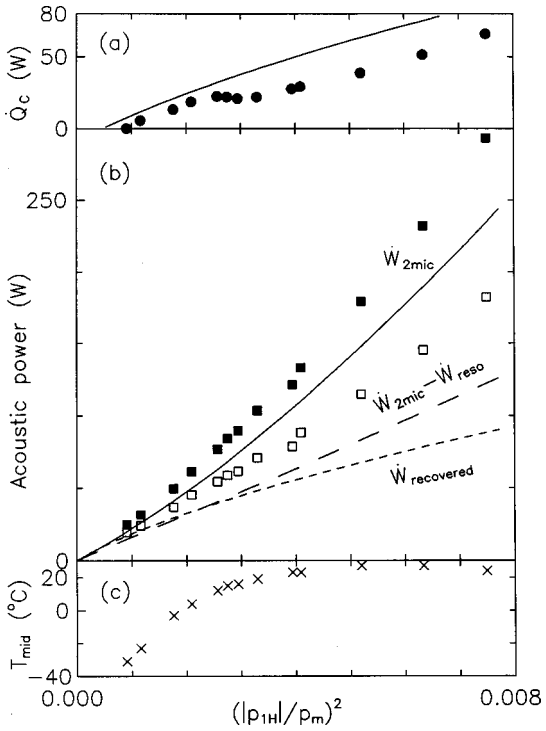

FIG. 13. Powers and mid-regenerator temperature at $T_C = -55\,^{\circ}\mathrm{C}$, as a function of pressure amplitude, with final configuration with jet pump and small extra resistance. $T_H = 13\,^{\circ}\mathrm{C}$ throughout. The symbols have the same meaning as in Fig. 12. (a) Cooling power. (b) Acoustic powers. (c) Mid-regenerator temperature.

and Gedeon's streaming in the extra resistance below the jet pump. Additional evidence that such components are contributing significantly to streaming is provided by the steep slope $d\dot{Q}_C/dT_C$ observed in our original, ''empty'' configuration and discussed below Eq. (17), which suggests that the ''empty'' configuration had a large nonzero $\Delta p_{2,0}$ across the regenerator, with its sign driving $U_{2,0}$ in the same direction as $1/2\,\mathrm{Re}[p_1 \tilde{U}_1]$.

The sensitivity of $\dot{M}$ to small details, illustrated in Figs. 11 and 13(a), suggests that practical use of a jet pump to suppress streaming in this type of refrigerator will require convenient adjustability in the jet pump or in some other $\dot{M}$-controlling part of the acoustic network.

IV. CONCLUSIONS

The $\dot{M} \simeq 0$ operating points in Fig. 13 are the most efficient operating points observed in these measurements. At the points near the relative maximum in cooling power in Fig. 13(a), the experimental coefficient of performance $\mathrm{COP} = \dot{Q}_C/\dot{W}_{2\mathrm{mic}} = 0.29$, so that the second-law efficiency is 9%. [The second-law efficiency is $\mathrm{COP}/\mathrm{COP}_{\mathrm{Carnot}}$, where $\mathrm{COP}_{\mathrm{Carnot}} = T_C/(T_H - T_C)$.] This is not as high as today's best traditional orifice PTRs[17] (10%–20% of Carnot) or standing-wave thermoacoustic refrigerators[33] (20% of Carnot), but it is high enough to show that this type of refrigerator has promise. If we deduct the calculated resonator dissipation from the experimental $\dot{W}_{2\mathrm{mic}}$, we obtain a second-law efficiency of 13%. We are confident that we can design much more efficient systems, based on the lessons we've described in this paper. For example, in our present refrigerator the inertance should have had a larger diameter and more streamlined ends; constraints of our existing hardware prevented such apparently straightforward modifications. Even simple improvements to our thermal insulation and use of a tapered pulse tube[8] could improve performance significantly, by increasing net cooling power with no cost to acoustic power.

We have discovered no reasons to doubt Ceperley's conclusion that efficiencies much greater than half of Carnot's are possible; we believe he was correct to suggest that traveling-wave refrigerators offer the potential for excellent performance with the simplicity of no moving parts. However, in addition to following Ceperley's ideas, it is vital to suppress time-averaged mass flux through such a refrigerator, and to use a thermal buffer column such as the pulse tube of a traditional PTR.

These same principles also apply to engines, which will be the subject of a paper in the near future.

Much more overall exploration remains to be done. Here, we have investigated the transmission-line configuration briefly, and the lumped boost configuration in more detail. It seems likely that other traveling-wave configurations can be discovered; they may offer advantages in efficiency or size. We used a balloon and a jet pump to suppress streaming; again, it seems likely that other, possibly better methods remain to be discovered. Quantitative understanding of all the sources of $\Delta p_{2,0}$ in the network will also be challenging.

In addition to these general research issues, considerable engineering effort will be required to determine how such techniques might impact specific applications such as cryogen liquefaction, cooling of superconducting electronics, or food refrigeration.

ACKNOWLEDGMENTS

This work has been funded by the Offices of Basic Energy Sciences and Fossil Energy in the U. S. Department of Energy. We thank Vince Kotsubo for useful conversations regarding the diagnosis and suppression of streaming.

[1] R. Radebaugh, ''A review of pulse tube refrigeration,'' Adv. Cryog. Eng. **35**, 1191–1205 (1990).
[2] P. Kittel, ''Ideal orifice pulse tube refrigerator performance,'' Cryogenics **32**, 843–844 (1992).
[3] Cryenco, Inc., 3811 Joliet, Denver, CO 80239.
[4] G. W. Swift, ''Thermoacoustic natural gas liquefier,'' in Proceedings of the DOE Natural Gas Conference, Houston, TX, March 1997.
[5] A. Bejan, *Advanced Engineering Thermodynamics* (Wiley, New York, 1997), 2nd ed.
[6] P. H. Ceperley, ''Gain and efficiency of a short traveling wave heat engine,'' J. Acoust. Soc. Am. **77**, 1239–1244 (1985), and references therein.
[7] G. W. Swift, M. S. Allen, and J. J. Wollan, ''Performance of a tapered pulse tube,'' to be published in the Proceedings of the 10th International Cryocooler Conference, Monterey CA, May 1998.
[8] J. R. Olson and G. W. Swift, ''Acoustic streaming in pulse tube refrigerators: Tapered pulse tubes,'' Cryogenics **37**, 769–776 (1997).
[9] R. Radebaugh, personal communication.
[10] D. Gedeon, ''DC gas flows in Stirling and pulse-tube cryocoolers,'' in *Cryocoolers 9*, edited by R. G. Ross (Plenum, New York, 1997), pp. 385–392.
[11] L. E. Kinsler, A. R. Frey, A. B. Coppens, and J. V. Sanders, *Fundamentals of Acoustics* (Wiley, New York, 1982).

[12] B. J. Huang and C. W. Lu, ''Dynamic response of regenerator in cyclic flow system,'' Cryogenics **33**, 1046 (1993).
[13] B. J. Huang and C. W. Lu, ''Linear network analysis of regenerator in a cyclic-flow system,'' Cryogenics **35**, 203 (1995).
[14] G. W. Swift and W. C. Ward, ''Simple harmonic analysis of regenerators,'' J. Thermophys. Heat Transfer **10**, 652–662 (1996).
[15] J. H. Xiao, ''Thermoacoustic theory for cyclic flow regenerators. Part I: Fundamentals,'' Cryogenics **32**, 895 (1992).
[16] For an ideal gas, specific heat c_p is constant and the hydrodynamic contribution to the time-averaged energy flux is $\overline{\rho(t)c_pT(t)U(t)}$, where the overbar denotes time average. If the gas is in perfect thermal contact with the regenerator matrix, $T(t)\equiv T_m$ is constant. If also the time-average mass flux $\overline{\rho(t)U(t)}$ through the regenerator is zero, then $\overline{\rho(t)c_pT(t)U(t)}=0$.
[17] R. Radebaugh, ''Advances in cryocoolers,'' in *Proceedings of the 16th International Cryogenic Engineering Conference/International Cryogenic Materials Conference* (ICE16/ICMC) (Elsevier Science, Oxford, 1997), pp. 33–44.
[18] S. W. Zhu, S. L. Zhou, N. Yoshimura, and Y. Matsubara, ''Phase shift effect of the long neck tube for the pulse tube refrigerator,'' in *Cryocoolers 9*, edited by R. G. Ross (Plenum, New York, 1997), pp. 269–278.
[19] S. Zhu, P. Wu, and Z. Chen, ''Double inlet pulse tube refrigerators: An important improvement,'' Cryogenics **30**, 514 (1990).
[20] P. M. Morse and K. U. Ingard, *Theoretical Acoustics* (McGraw–Hill, New York, 1968) Chap. 6.2.
[21] D. L. Gardner and G. W. Swift, ''Use of inertance in orifice pulse tube refrigerators,'' Cryogenics **37**, 117–121 (1997).
[22] Briefly, similitude requires that reduction of all dimensions of the apparatus by a factor of 2 is accompanied by a reduction of all thermophysical length scales in the gas by a factor of 2. Here, the relevant thermophysical length scales are the acoustic wavelength $\lambda=a/f$ and the viscous penetration depth $\delta_\nu=\sqrt{\mu/\pi f\rho}$. Reducing these lengths by a factor of 2 determines the frequency and pressure necessary to make argon in the half-scale apparatus *similar* to helium in the full-scale apparatus. For a more complete treatment (discussing the temperature dependence of μ and K, similarity of Prandtl number, and other effects), see Ref. 23.
[23] J. R. Olson and G. W. Swift, ''Similitude in thermoacoustics,'' J. Acoust. Soc. Am. **95**, 1405–1412 (1994).
[24] The hydraulic radius is the ratio of gas volume to gas–solid contact surface area.
[25] W. M. Kays and A. L. London, *Compact Heat Exchangers* (McGraw-Hill, New York, 1964).
[26] A. M. Fusco, W. C. Ward, and G. W. Swift, ''Two-sensor power measurments in lossy ducts,'' J. Acoust. Soc. Am. **91**, 2229–2235 (1992).
[27] G. W. Swift, ''Analysis and performance of a large thermoacoustic engine,'' J. Acoust. Soc. Am. **92**, 1551–1563 (1992).
[28] W. C. Ward and G. W. Swift, ''Design environment for low amplitude thermoacoustic engines (DeltaE),'' J. Acoust. Soc. Am. **95**, 3671–3672 (1994). Fully tested software and users guide available from Energy Science and Technology Software Center, U. S. Department of Energy, Oak Ridge, TN. To review DeltaE's capabilities, visit the Los Alamos thermoacoustics web site at http://rott.esa.lanl.gov/. For a beta-test version, contact ww@lanl.gov (Bill Ward) via Internet.
[29] M. Iguchi, M. Ohmi, and K. Maegawa, ''Analysis of free oscillating flow in a U-shaped tube,'' Bull. JSME **25**, 1398 (1982).
[30] W. L. M. Nyborg, ''Acoustic streaming'' in *Physical Acoustics*, edited by W. P. Mason (Academic, New York, 1965), Vol. IIB, p. 265.
[31] R. W. Fox and A. T. McDonald, *Introduction to Fluid Mechanics* (Wiley, New York, 1985).
[32] V. L. Streeter, *Handbook of Fluid Dynamics* (McGraw-Hill, New York, 1961)
[33] S. L. Garrett, J. A. Adeff, and T. J. Hofler, ''Thermoacoustic refrigerator for space applications,'' J. Thermophys. Heat Transfer **7**, 595–599 (1993).